Calcite and carbocernaite exsolution and cotectic textures in a Sr,*REE*-rich carbonatite dyke from Rajasthan, India

F. WALL

Department of Mineralogy, The Natural History Museum, Cromwell Road, London SW7 5BD, U.K.

M. J. LE BAS

Department of Geology, The University, Leicester LE1 7RH, U.K.

AND

R. K. SRIVASTAVA

Department of Geology, M.L. Sukhadia University, Udaipur 313001, India

Abstract

A carbonatite dyke from the Sarnu–Dandali alkaline complex, Rajasthan, India, contains a remarkable suite of rare earth, strontium-rich minerals with spectacular primary textures.

Sr, Mn-rich calcite in the outer 5 mm of the dyke contains exsolved lamellae of carbocernaite, $(Ca,Na)(Sr,Ce,Ba)(CO_3)_2$, orientated parallel to its twin and cleavage planes. The amount of exsolved carbocernaite increases away from the dyke margin as the Sr content of the calcite increases to a maximum 13 wt.%. Sr levels as high as this in calcite have previously been recorded only in experimental work. The carbocernaite exsolution suggests that Sr-rich calcium carbonate can be a host for major amounts of *REE* in carbonatite magma.

Separated by a sharp internal boundary, is a complex possibly cotectic intergrowth of carbocernaite and Sr-rich calcite with late Ca-rich strontianite (19 wt.% CaO). Other minerals in the dyke include baryte, pyrrhotite, alabandite, sphalerite and occasional bastnäsite–(La) and thorite. Bands of late britholite-(Ce) traverse the dyke.

The host rock for the dyke is fenitized melanephelinite which is itself traversed by narrow, <1 mm, carbonatite veins beleived to predate the carbonatite dyke. Allanite, britholite-(Ce) and rare monazite-(Ce), developed at the boundary between the carbonatite dyke and the fenite, may have been produced by a reaction between the dyke and the wall rock, or may be related to the later britholite mineralisation.

The textures and mineral compositions indicate primary crystallisation. They are unique amongst rare earth-rich carbonatites which are usually late-stage phenomena with signs of secondary alteration.

Comparison with experimental data available for the calcite–strontianite system suggests conditions of 500 °C and 2 kbar for coexisting Sr-rich calcite and Ca-rich strontianite. A smaller scale intergrowth of calcite containing only 2.9 wt.% SrO and coexisting Ca-strontianite may correspond to a further unmixing at 350 °C and 2 kbar. Since no experimental data are available for a calcite–carbocernaite–strontianite system, mineral chemistries and the interpreted sequence of crystallisation have been used to construct a hypothetical phase diagram.

KEYWORDS: carbonatite, Rajasthan, *REE*, strontian calcite, carbocernaite, strontianite, britholite-(Ce), cotectic, exsolution, micrographic intergrowth.

Introduction

THE alkaline igneous rocks of the Sarnu-Dandali area, Barmer District, Rajasthan, India, consist of a suite of alkali pyroxenites, melanephelinites, ijolites, and micro-melteigites cut by thin dykes of carbonatite with later thin dykes of foidal syenite and phonolite (Chandrasekaran *et al.*, 1990). The

Mineralogical Magazine, September 1993, Vol. 57, pp. 495–513

assemblage occurs as scattered outcrops surrounded by wind-blown sands and covers an area of *ca.* 200 km^2. The purpose of this paper is to describe and interpret the 25 mm wide marginal portion of one of the carbonatite dykes. This has been found to contain an assemblage of *REE*, Sr and Mn-rich carbonates that is remarkable both for its unique mineral compositions and for its spectacular mineral textures. The dyke is believed to be about 100 mm wide, although only the outer 25 mm could be sampled. It penetrates a melanephelinite (described by Chanadrasekaran *et al.*, 1990, samples C251 and C253) and has fenitized its surrounding host rock. The carbonatite suite as a whole has not yet been studied in detail but it is known that other carbonatites are also *REE*-rich.

Analytical methods

Whole-rock analysis for major elements was made by X-ray fluorescence analysis at the University of Leicester with an ARL 8420 dual goniometer wavelength dispersive spectrometer using a 3 kw Rh X-ray tube. The data were processed using ARL 386 software. The trace elements were similarly analysed but using 3 kw Rh and W tubes on the Philips PW1400 X-ray spectrometer. Duplicate analyses were performed using combined atomic absorption and spectrophotometric methods as described by Srivastava (1977). CO_2 was determined gravimetrically.

Electron microprobe analysis and backscattered electron imagery were carried out at The Natural History Museum, London. A Hitachi S2500 scanning electron microscope equipped with a Link AN1055/S energy-dispersive analysis system (operated at 15 kV and 1 nA on a vanadium calibration standard) was used for preliminary analyses and to check beam sensitive material. A Cambridge Instruments Microscan 9 wavelength-dispersive microprobe (operated at 20 kV and 25 nA specimen current on the Faraday cage) was used for the analysis of *REE*-minerals. A set of *REE* silicate glasses, synthesised at the University of Edinburgh, were used as standards for the rare earth elements and empirical correction factors were used for the interference where necessary. Matrix correction was by ZAF.

The identities of two of the minerals, calcite and carbocernaite, were checked by X-ray Debye-Scherrer powder diffraction.

Whole-rock chemistry

The whole-rock chemistry was determined before it was appreciated that the dyke was heterogeneous and therefore the analysis represents the whole of the marginal portion of sample C254, excluding the fenite and the calcite veins.

In terms of its major oxide constituents (Table 1), the carbonatite has a composition transitional between that of sövite and ferrocarbonatite, with some unusual features. (1) The MnO content is high at nearly 3%. However, MnO is known to increase with the fractionation of carbonatite (Clarke *et al.*, 1992, in press). (2) The high sum of Na_2O + K_2O at >1% is abnormal because there are no feldspars, micas, amphiboles or pyroxenes in the carbonatite. Carbocernaite is a possible host mineral for the sodium but the host for the potassium is not known. (3) Elements usually present in low

TABLE 1
Whole rock analysis of carbonatite dyke

	C254
	wt%
SiO_2	2.27
TiO_2	0.06
Al_2O_3	0.35
Fe_2O_3(T)	4.65
MnO	2.78
MgO	0.88
CaO	39.30
Na_2O	0.75
K_2O	0.63
P_2O_5	0.76
LOI	34.00
Total	86.43
Total including trace elements	101.00
	ppm
V	1
Cr	6
Ni	17
Zn	3400
Ga	7
Rb	1
Sr	53000
Y	133
Zr	1
Nb	227
Ba	11830
La	22850
Ce	27750
Nd	4950
Th	34

Fe_2O_3(T) = total iron as Fe_2O_3
LOI = loss on ignition

quantities in carbonatite are present in major proportions, *viz. ca.* 6% *REE*, 5% SrO and 1.2% BaO, and this prompted the electron microscope search for the *REE*-bearing host minerals.

The multi-element variation diagram (Fig. 1), in which the Sarnu carbonatite is compared with the average carbonatites of Woolley and Kempe (1989), shows that the Sarnu carbonatite has the chemical character of a typical carbonatite that has undergone fractional crystallisation, as shown by Clarke *et al.* (1992). It has relatively high normalised ratios for La, Ce, Nd and Ba but a slightly lower ratio for Sr. Nb, Zr and Ti have smaller ratios as appropriate to elements that occur in minerals commonly fractionated early from carbonatite magma, i.e. pyrochlore, zircon and titaniferous magnetite. P is also usually much reduced in fractionated carbonatite owing to the early precipitation of apatite, the P content of the Sarnu carbonatite is only slight lower than that for the average carbonatites plotted on Fig. 1. This is surprising in view of the lack of apatite in the dyke. However, electron microprobe analysis revealed an abundance of the mineral britholite-(Ce) (the silicate analogue of apatite) which contains minor P as well as rare monazite-(Ce) (30 wt.% P_2O_5) and probable daqingshanite.

Mineralogy and petrology

Hand specimen

In hand specimen the boundary between dark grey fenitized melanephelinite and the light grey carbonatite dyke is sharp. Immediately adjacent to the fenite there is a 5 mm wide band of coarse-grained carbonatite which is darker in colour than the rest of the carbonatite due to the presence of a greater concentration of <0.5 mm opaques. Beyond this band the carbonatite is medium-grained and apparently uniform.

Thin section

At first sight, under an optical microscope, the carbonatite appears to be composed almost

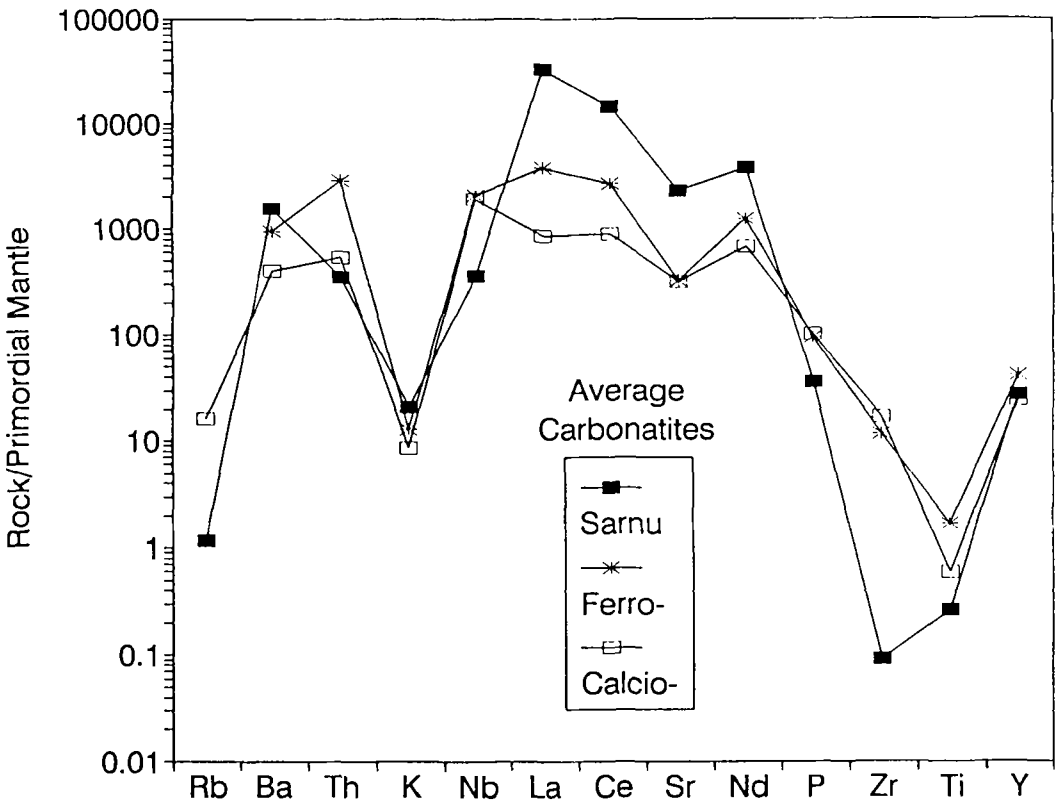

FIG. 1. Multi-element variation diagram, normalised to primordial mantle of Wood *et al.* (1979), to compare the Sarnu dyke C254 (Table 1) with average calciocarbonatite and ferrocarbonatite of Woolley and Kempe (1989).

entirely of calcite with rare isolated crystals of opaque minerals and faint outlines of possibly more complicated textures. However, the texture of the carbonatite is beautifully displayed under the scanning electron microscope by backscattered electron imagery of a polished thin section (Fig. 2).

The main constituents of the carbonatite are strontian calcite, carbocernaite (Ca,Na)(Sr,Ce,-Ba)$(CO_3)_2$, britholite-(Ce) $(Ca_2Ce_3(SiO_4)_3$-(OH,F)), and calcian strontianite, plus minor baryte, pyrrhotite, sphalerite, alabandite (MnS), Fe-oxides and, probably, daqingshanite (Sr,Ca,-Ba,Ce)$_4(PO_4)(CO_3)_3$). In addition, an assemblage of allanite-(Ce), britholite-(Ce) and rare monazite-(Ce) is present at the boundary between the carbonatite dyke and the fenite.

The dyke is heterogeneous and, for clarity, the carbonatite and fenite have been divided into seven Areas, A–G (Fig. 2). The main features of each of these areas is described in Table 2 which may be used together with Figs 2, 3 and 4.

Mineral chemistry

Calcite in the dyke contains exceptionally high levels of Mn and Sr (Table 3). Values for MnO range from 3.15 to 4.34 wt.% and SrO ranges from 2.9 to an unprecedented 13 wt.%. These figures can be set against values normally reported from carbonatites of about 1–2 wt.% SrO and 1 wt.% MnO. It is possible that the Sr and Mn could be in an exsolved phase and not actually in the calcite structure. That this could be a microscopic phase, is largely discounted by the uniform backscattered coefficient of areas much larger than the spatial resolution of the electron microprobe and an XRD confirmation of calcite. However, there is still a small possibility that cryptocrystalline exsolution textures may be present and a transmission electron microscopy study would be extremely useful.

The Sr content of calcite increases from Area A to Area B concomitant with the increasing amount of exsolution; compare analyses 1 and 2 in Table 3 which contain 4.98 and 10.77 wt.% SrO respectively.

Compositions in Area C are also variable. Much of the calcite is high in Sr and Mn and, therefore, similar to calcite in the exsolved crystals of Area B (analysis 3 in Table 3), but in contrast, calcite in the centre of crystals which contain a calcian strontianite–calcite small-scale intergrowth (Fig. 3*d*) contains much less Sr (analysis 4, Table 3).

Calcite in the narrow veins penetrating the fenite is of a (relatively) low Sr, low Mn variety (analysis 6, Table 3) and is much more like a 'normal' carbonatite calcite.

Chemical trend across Areas A and B. The apparent chemical trend across the outer part of the dyke (i.e. Areas A and B) shown by the changing Sr content of calcite and the increase in the amount of exsolved carbocernaite was tested by making a series of ten raster analyses on areas of about 120 × 150 μm, chosen to cover both uniform calcite and exsolution features with as few impurities as possible. The results (Table 4) were used to construct plots of Ca and Sr versus the degree of exsolution on an arbitrary scale of 1 to 5 based on the size of the carbocernaite lamellae seen on a backscattered electron image (Fig. 4). These graphs confirm that there is a general trend in the 'pre-exsolution composition' of the carbonate. Ca decreases and Sr increases with increasing distance from the dyke margin. Thus, the crystals at the edge of the dyke are not simply frozen equivalents of the crystals with the large exsolution lamellae.

Calcian strontianite, whether as blebs in Sr-rich calcite, narrow partial mantles on large carbocernaite crystals (Fig. 3*c*), or strontianite in Sr-poor calcite (Fig. 3*d*), varies little in composition throughout Area C. The Ca content of the strontianite is exceptionally high with nearly 20 wt.% CaO, equivalent to 52 mol.% Ca (analyses 7, 8 and 9 in Table 3).

Experimental data for calcite and strontianite. Although the Sr levels in the calcite and the Ca levels in strontianite are higher than any previously reported in natural rocks, such compositions have been synthesised in experimental studies. The effects of Sr substitution on the calcite (trigonal)–strontianite (orthorhombic aragontie structure) equilibrium have been investigated by Carlson (1980) and equilibria in the Sr–Ba–Ca carbonate system have been studied by Chang and Brice (1972). In order to compare the minerals from Sarnu with experimental results it is necessary to be satisfied that the impurities such as Ba, Mn and *REE* will not have a major effect on the phase boundaries. Chang and Brice (1972) demonstrated that low levels of barium have very little effect on calcite-aragonite equilibria. The effect of the presence of Mn and *REE* (up to 0.38 wt.% in strontianite, Table 3) is not known, but in order to fit the observed compositions to the experimental data of Carlson (1980), *REE* have been assigned to the Sr site and Mn to the Ca site (see Table 3, mol.%). Fig. 5*a* shows that the observed compositions of the coexisting neighbouring calcite and strontianite at the edge of carbocernaite in Area C (Fig. 3*c*) plot onto the isothermal section at 500 °C at about 2 kbar. No

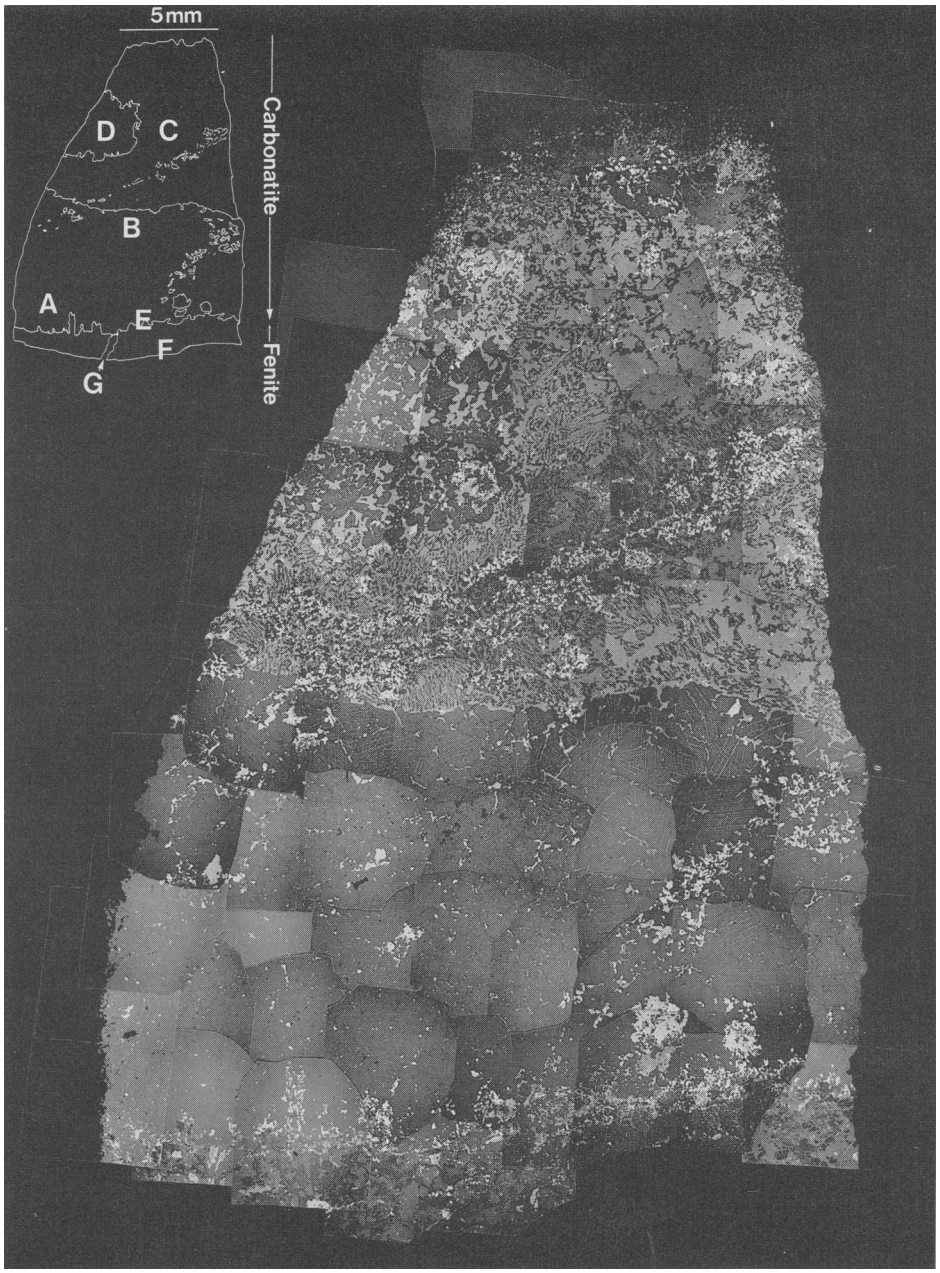

FIG. 2. Composite backscattered electron micrograph of a polished thin section of Sarnu carbonatite C254. Area A—strontian calcite (dark grey), some britholite-(Ce) (white) and opaques (white). See also Area E. Area B—strontian calcite (dark grey), lamellae and interstitial crystals of carbocernaite (mid-grey), small equant opaques (white) and concentrations of britholite-(Ce) (white). Area C—intergrown carbocernaite (mid-grey) and calcite (dark grey); concentration of britholite-(Ce) at centre of this area, approximately parallel with the dyke margin (white); anhedral baryte at margins of large carbocernaite crystals (white). See Fig. 3 for details. Area D—calcite (dark grey) with lamellae, and interstitial crystals, of carbocernaite (mid grey) and concentrations of britholite-(Ce) (white). Area E—fenite–carbonatite boundary: on carbonatite side—calcite (dark grey), allanite-(Ce) (mid-grey) and britholite-(Ce) (white). On fenite side—albite (dark grey) and phlogopite (grey). Area F—fenite. Major constituents are albite and phlogopite. Area G—calcite vein (starts from here but not visible on backscattered image).

TABLE 2 Petrology of the Sarnu carbonatite dyke, C254

Minerals	Comments
	Area A calcite near fenite contact
	Outer 2-4 mm of the dyke
Sr-Mn-rich calcite	Large euhedral (≈ 1mm) crystals. Uniform backscattered coefficient on Fig. 2 but, under higher magnification most crystals contain aligned "blebs" (Fig. 4) which are too small for electron microprobe analysis. Number and size of blebs increases with increasing distance from the dyke margin, grading into Area B.
Britholite-(Ce))	Irregular band cuts obliquely across Areas A and B (white, and shown on the inset, in Fig. 2). Concentrated between the large calcite crystals and often within the interstitial carbocernaite.
alabandite) phyrrotite)	Small, equant crystals scattered throughout the calcite. Minor phases.
	Area B Calcite crystals with large carbocernaite lamellae
	1-3 mm wide
Sr-Mn-rich calcite	Large euhedral crystals, slightly larger than in Area A Crystals contain large exsolution lamellae of carbocernaite, orientated along the calcite cleavages and twin planes {0112} and {1011}, visible on Fig. 2 (see also Fig. 3a). In transmitted light, the lamellae are difficult to distinguish from the calcite, and under crossed polars they are sometimes seen to be in optical continuity with it.
carbocernaite	Lamellae in calcite (see above) and 100 μm crystals interstitial to the calcite.
britholite-(Ce))	Irregular band cuts obliquely across Areas A and B (white, and shown on the inset, in Fig. 2). Concentrated between the large calcite crystals and often within the interstitial carbocernaite.
alabandite) pyrrhotite)	Small, equant crystals scattered throughout the calcite in both areas. Minor phases.
	Area C "cotectic" intergrowth of calcite and carbocernaite
	Complex intergrowth of carbocernaite and strontian calcite reminiscent of a "symplectic" or micrographic" texture (Figs. 2 and 3b,c,d). Sharp boundary with Area B defined by a line of carbocernaite (Fig. 2).
carbocernaite	Identity confirmed by XRD. Crystals vary in size from 150 μm to 1.5 mm. Not zoned. Contain occasional inclusions of bastnäsite-(La) (Fig. 3b and Table 4) and thorite. Large crystals grade into the "micrographic" texture. In places the carbocernaite is so narrow and elongate as to resemble a spinifex quench texture.
Sr-Mn-rich calcite	Contains numerous <4 μm blebs of carbocernaite, calcian strontianite (Fig. 3c).
Ca-rich strontianite	Anhedral blebs in calcite and narrow partial mantles of the same strontianite at the edge of the large carbocernaite crystals (Fig.3c). Second smaller scale intergrowth in some calcite crystals consisting of strontianite and calcite (Fig. 3d).
baryte	At margins of carbocernaite, anhedral 60 x 20 μm crystals (Fig. 3d). Contains 3.6 wt% SrO, traces of Na and Ca.
dagingshanite	$((Sr,Ca,Ba,Ce)_4(PO_4)(CO_3)_3)$. Small (20 μm) crystals at the edge of carbocernaite (Fig. 3d). Composition is very close to that of strontium-rich dagingshanite described by Appleton et al. 1992 from the Nkombwa carbonatite, Zambia.
alabandite) pyrrhotite)	Unevenly distributed small, equant, associated crystals of pyrrhotite (F 60.9, S 38.5 wt%) and alabandite (Mn 56.4, Fe 7.6, S 36.5 wt%), similar to those seen in Areas A and B. Also pyrrhotite at edges of large carbocernaite crystals.
sphalerite	Larger (300 μm) but rarer subhedral grains at grain boundaries. High Fe at 13.9 wt% $(Zn_{1.1}Fe_{0.46}Mn_{0.42}S_2)$.
britholite-(Ce))	Band cuts obliquely across the area, same as in Areas A and B.
	Area D calcite with lamellae of carbocernaite and much interstitial carbocernaite
	One centimetre into the dyke
carbocernaite) calcite)	Texture similar to Area B (Fig. 2) but proportion of interstitial carbocernaite between the calcite is greater and boundary between Areas D and C is less obvious than the boundary between Areas B and C. Proportion of calcite to carbocernaite is approximately 2:1.
britholite-(Ce))	Again within the interstitial carbocernaite.
	Area E fenite-carbonatite boundary
	Hand specimen boundary is sharp
britholite-(Ce)) allanite-(Ce)) monazite0(Ce))	In thin section the boundary is marked by aggregates of britholite-(Ce) pleochroic (Ce) and rare monazite-(Ce) which lie just within the carbonatite (Table 6 nos 8, 9 and 10, and Fig. 2). May be fragments of the wall rock which have become incorporated into the carbonatite dyke and have reacted with it. No surviving "fenite" mineral phases were detected.
calcite	Surrounding these aggregates is described in Area A.
	Area F fenite
albite	Major phase. Euhedral turbid 40 x 400 m crystals. Ab97, Table 7.
phlogopitic mica	Major phase. Turbid brown anhedral grains up to 1 mm diameter. At margin with calcite vein (Area G) - mica is green, more magnesian and with lower Al_2O_3 content (Table 7) as typifies more strongly fenitized micas (Le Bas and Srivastasa, 1989).
opaques	Mainly concentrated in the phlogopite and ilmenite plus magnetite, the majority are about 10 μm in diameter but ranging up to 400 μm.
apatite	Occasional crystals. Contain about 1 wt% SrO but no detectable REE (Table 7 no. 6).
	Area G calcite vein in fenite
	The fenite is cut by a number of fine calcite veins. Largest vein is of variable width, maximum 0.2 mm, and penetrates the fenite from the carbonatite dyke.
calcite	Sr-Mn rich but much less so than the calcite from the dyke (Table 3 no. 6). No exsolution.
magnetite)	Magnetite is rimmed by REE-rich titanite)an REE-rich titanite (Table 6) similar in composition to that described in Skye granites by Exley (1980).
apatites	Have REE- and Sr-rich rims and also occasional tiny monazite-(Ce) crystals at their margins (Table 7).

other experimental conditions produced these two compositions. This temperature is realistic for carbonatite (Wyllie, 1989), and we believe that the pressure is also consistent with the

TABLE 3
Electron microprobe analyses of calcite and strontianite

	CALCITE										STRONTIANITE			
Area	A near fenite no carbocernaite lamellae		B in crystal with large lamellae of carbocernaite		C intergrown calcite/ carbocernaite		C intergrown calcite/ strontianite Fig. 3d	D		G vein in fenite	C intergrown calcite/ carbocernaite		C At edge of large carbocernaite crystal Fig. 3c	C intergrown calcite/ strontianite Fig. 3d
Number	1		2		3		4	5		6	7		8	9
Analysis	average of 4	sd	average of 6	sd	average of 5	sd	SAR15	average of 2	sd	FW33	average of 3	sd	ZA	SAR14
Na_2O	0.20	0.12	-		-		-	-		-	-		0.30	-
MgO	0.28	0.06	0.49	0.09	0.41	0.08	0.77	0.50	0.06	0.39	-		-	-
CaO	47.15	2.55	45.37	1.18	45.44	1.39	50.03	43.12	0.92	51.93	18.83	0.27	19.09	16.76
MnO	3.69	0.7	4.20	0.44	3.15	0.23	4.34	4.14	0.29	2.23	-		-	0.58
FeO(T)	0.37	0.09	-		-		0.32	0.24	0.19	0.59	-		-	-
SrO	4.98	0.59	10.77	1.29	9.49	1.91	2.89	13.12	0.27	2.39	46.78	0.28	47.76	43.99
BaO	-		0.79	0.16	0.93	0.48	-	0.88	0.29	-	1.52	0.07	0.22	2.53
La_2O_3	-		-		-		-	-		-	-		0.14	-
Ce_2O_3	-		0.42	0.17	-		-	-		-	-		0.24	-
TOTAL	56.67		62.03		59.42		58.35	61.99		57.53	67.13		67.75	63.86
wt% CO_2*	41.48		42.04		40.94		43.79	40.95		43.58	28.08		28.71	26.34
total*	98.15		104.07		100.35		102.14	102.94		101.11	95.21		96.46	90.20
mol% Ca+ Mn+Mg	95.47		92.15		92.97		97.74	90.22		97.66	52.62		52.18	51.30
mol% Sr+Ba +REE+Na	3.30		7.85		7.03		1.82	9.43		1.51	47.38		46.33	48.70

FeO(T) = total iron as FeO
* = CO_2 calculated by stoichiometry and corresponding total
sd = standard deviation
\- = below detection limits
For further information on Areas see text and Fig. 2
Number 9 is included despite the low calculated total,
to give the Ca/Sr ratio of strontianite coexisting with 4.

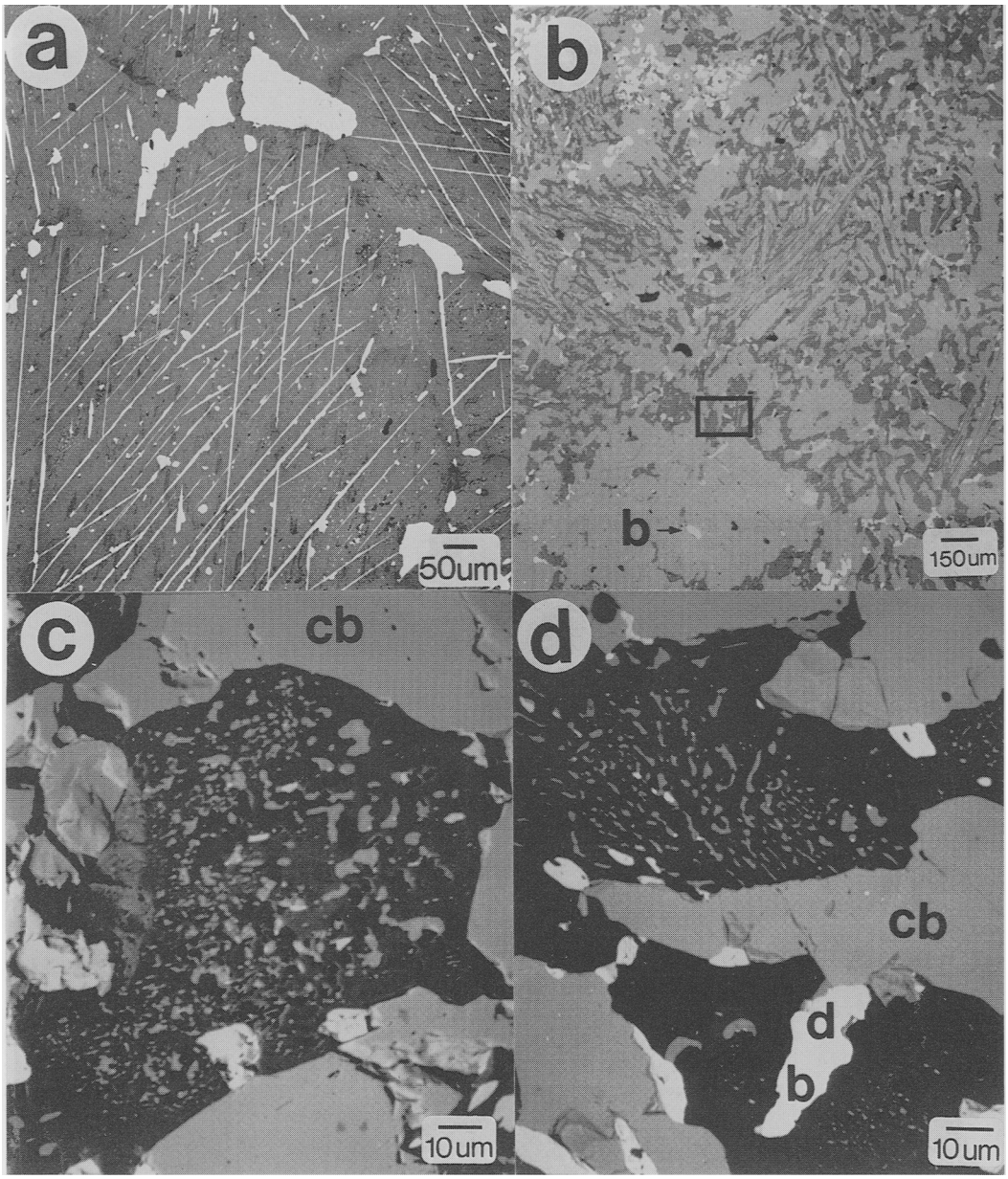

FIG. 3. Backscattered electron micrographs. (*a*) In Area B. Lamellae of carbocernaite (white) in calcite crystal (mid-grey) with interstitial carbocernaite (white). Other small (<10 μm) white crystals within the calcite are alabandite and pyrrhotite. (*b*) Area C. Carbocernaite (mid-grey)—calcite (dark grey) intergrowth. Cluster of white crystals is britholite-(Ce). Note also bastnäsite inclusion (b). (*c*) Area C. Detail of area just to left of Fig. 3*b*. Carbocernaite (cb), strontianite (slightly darker grey, to the left of carbocernaite) and calcite (black) with intergrown carbocernaite and strontianite. (*d*) Area C. Detail of area outlined on Fig. 3*b*. Carbocernaite (mid-grey, one crystal marked cb) with late dagingshanite (d) and baryte (b). Other white crystals are also baryte. The upper half of the photo contains an example of the small scale strontianite (mid-grey)—'low Sr-calcite' (black) intergrowth. See Table 3 for analyses. The lower half of the photo has 'high Sr-calcite' (black).

TABLE 4

Bulk electron microprobe analyses of individual crystals in Areas A and B, i.e. the analyses include both the calcite and the lamellae

Anal. No.	1	2	3	4*	5	6	7	8*	9	10
Magnification	x700	x700	x700	x700	x700	x700	x700	x700	x200	x700
Exsolution	very little	little	little	fine	fine	fine	medium	coarse	coarse	coarse
Type of exsolution	1	2	2	3	3	3	4	5	5	5
Na_2O	-	0.42	0.25	0.40	0.30	-	-	0.52	0.40	0.53
MgO	0.25	0.33	0.25	0.59	0.36	0.32	0.49	0.50	0.61	0.39
SiO_2	-	-	-	0.25	-	-	-	-	-	-
CaO	41.95	42.36	41.61	39.74	41.49	40.01	38.57	36.35	36.47	36.08
MnO	3.51	3.71	2.85	3.59	4.07	2.94	3.82	3.70	3.45	3.29
FeO(T)	0.37	0.48	0.41	0.61	-	0.77	1.38	1.53	0.99	0.43
SrO	5.73	5.16	7.49	7.26	6.74	10.18	8.82	10.93	11.09	11.76
BaO	-	-	-	-	-	-	0.77	0.59	-	-
La_2O_3	-	-	-	-	-	-	1.00	0.95	0.90	-
Ce_2O_3	0.72	-	-	0.84	0.75	1.11	0.91	1.42	1.41	1.04
SO_3	-	-	0.22	-	0.30	0.48	-	-	0.25	-
Total	52.53	52.46	52.87	53.27	53.71	55.32	55.75	56.48	55.31	53.51

FeO(T) = total iron as FeO

\- = below EDS detection limit of about 0.1 wt%

* = backscattered electron image on Fig. 4

amount of uplift and erosion likely to have occurred in the Sarnu area since the Cretaceous period.

The small-scale intergrowth of low-Sr calcite and calcian strontianite in Area C (Fig. 3*d*, analyses 4 and 9 in Table 3) is consistent with re-equilibration at a lower temperature when the amount of Sr that may have been accommodated in the calcite decreased greatly, but the amount of calcium in coexisting strontianite decreased very little. A best match is achieved on the 350–400 °C isothermal sections, again at about 2 kbar (Fig. 5*b*).

Carbocernaite, $(Ca,Na)(Sr,Ce,Ba)(CO_3)_2$, is a rare mineral. Here it has been distinguished from the chemically similar mineral, burbankite $(Na,Ca,Sr,Ba,Ce)_6(CO_3)_5$, by X-ray diffraction and by its stoichiometry which consistently gives a ratio of 6:6 cation : carbonate rather than the 6:5 ratio that would be expected for burbankite (Table 5). We believe that the analyses presented here are the first detailed microprobe analyses of carbocernaite in the literature.

The first description of carbocernaite was from a geological setting similar to that at Sarnu. It occurs in 0.5 to 1 mm wide dolomite–calcite carbonatite veins in pyroxenites and ijolites of the Vuorjärvi Massif, Kola Peninsula (Bulakh *et al.*, 1961), although the associated minerals are different. The chemistry of the Vuorjärvi carbocernaite is closely comparable with that at Sarnu. Values for (calculated) CO_2 are very similar. Strontium is higher at Sarnu than at Vuorjärvi, 21.4 wt.% compared with 12.43 wt.%, the high Sr content being compensated by lower Na, *REE* and Ca in the analyses reported here.

In Area B of the Sarnu dyke the exsolution lamellae and interstitial crystals of carbocernaite differ in composition (compare analyses 1 and 2 with 3 in Table 5), the former having lower Na and Sr and higher Ca. The wavelength-dispersive analyses of the exsolution lamellae given in Table 3 were checked on the energy-dispersive microprobe (which operates at a lower probe current and so has greater spatial resolution) to ensure that there was no contamination from the surrounding calcite. There is little variation within the carbocernaite of Area C which has an average composition close to that of the interstitial carbocernaite of Area B (compare analyses 4–9 and the average with analysis 3 in Table 5).

Throughout the dyke, carbocernaite is strongly

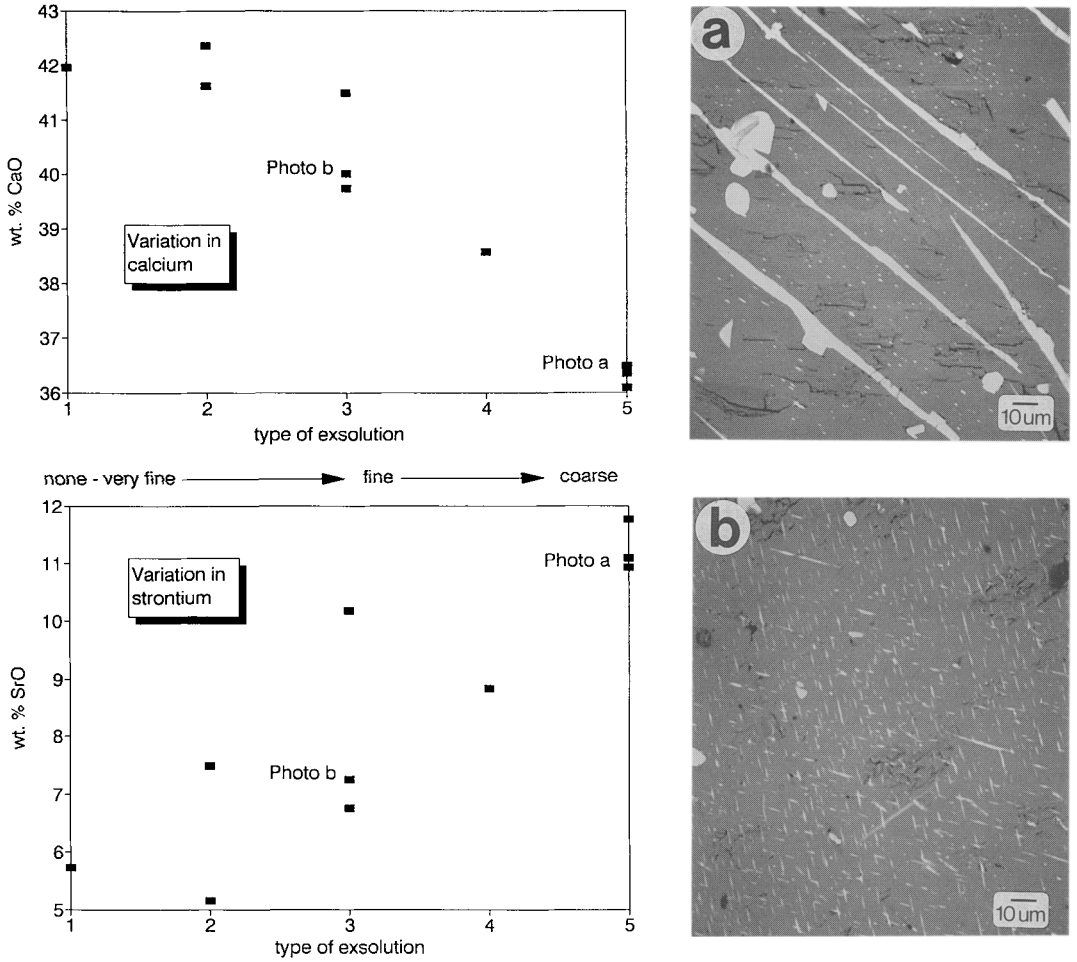

FIG. 4. Variation in CaO and SrO according to the type and amount of exsolved carbocernaite determined by analysing 120 × 150 μm areas such as those shown in Figs. 4*a* and *b*. The type of exsolution was classified on a scale of 1 (very little, fine exsolution) to 5 (abundant, large lamellae). For example, Fig. 4*a* show type 5 with large lamellae of carbocernaite (white) in calcite (dark grey). Note also the presence of fine blebs (white) in the background and larger rounded crystals of sulphide (white) (see also Figs. 2 and 3*a*). Fig. 4*b* is type 3 with abundant fine, aligned blebs and occasional rounded sulphides.

light rare earth (*LREE*) enriched with La being the dominant lanthanide in all cases except in some of the exsolved material (Table 5).

There are no experimental data available on the possible conditions of formation or phase relations of carbocernaite.

Britholite-(Ce) varies little in composition throughout the dyke (Table 6). It is always near the end member $Ca_2Ce_3(SiO_4)_3(OH,F)$.

Clark (1984) reports britholite-(Ce) as occurring chiefly in nepheline syenites and contact metasomatic deposits related to alkali syenites and granites. For example, britholite-(Ce) is present in place of the apatite in the more highly evolved rocks of the Shonkin Sag laccolith, Montana (Nash, 1972). Britholite-(Ce) thus appears to be a low-temperature mineral associated with late-stage or secondary events.

Rare earth patterns. All of the *REE* minerals in the Sarnu carbonatite are strongly light *REE*-enriched, as is characteristic of carbonatites. However, the light *REE*-enrichment is particularly strong and suggests a high degree of fractionation. This is illustrated by the greater enrichment in La relative to Ce and Nd of Sarnu compared with that of the average carbonatites on Fig. 1. The degree of light-*REE*-enrichment is such that only the light *REE* are detectable by

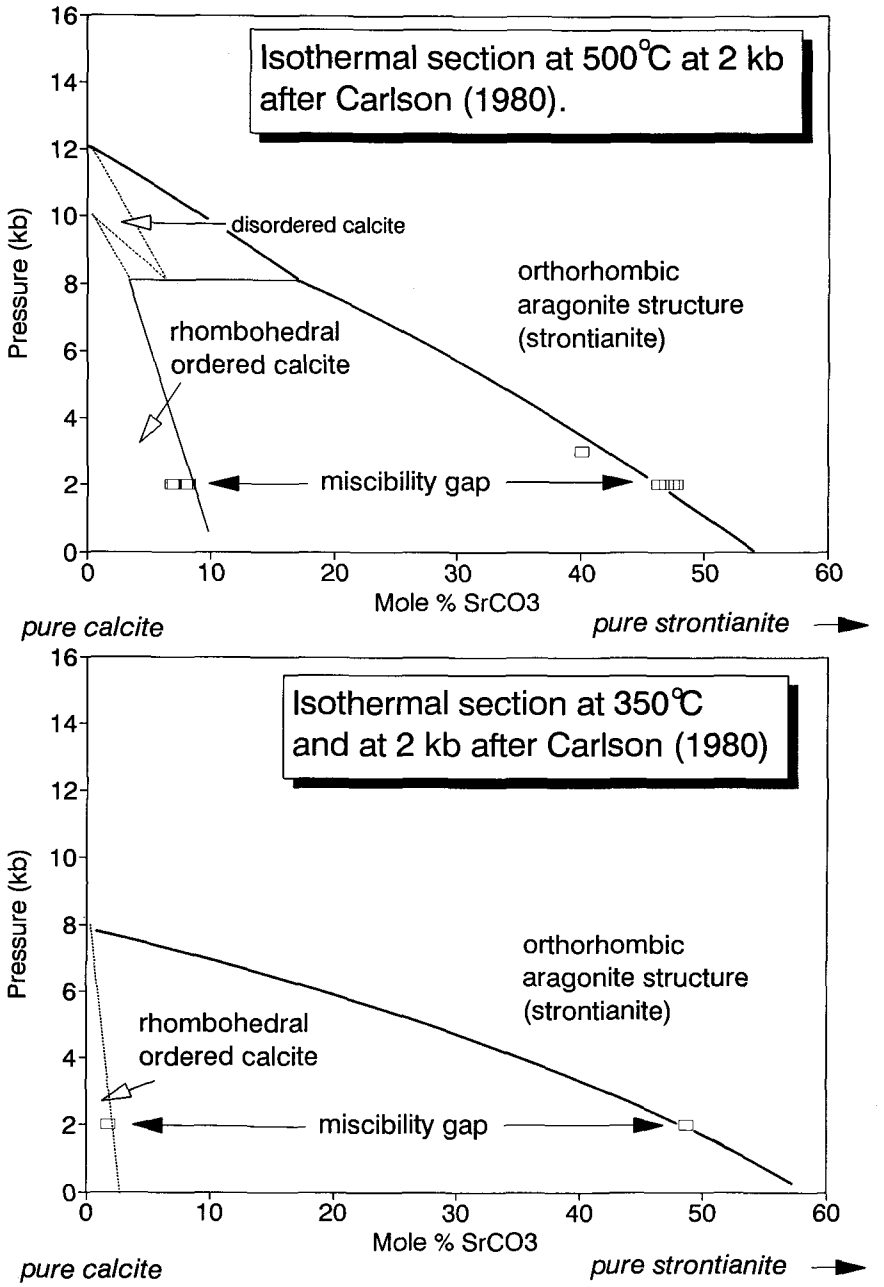

FIG. 5. Isothermal sections of 350 °C and 500 °C in the system calcite–Sr-aragonite (strontianite) after Carlson (1980). The low Sr-calcite–strontianite pairs plot best at 2 kbar on the 350 °C section, whereas the high Sr-calcite–strontianite pairs fit well onto the section at 500 °C at 2 kbar.

electron microprobe in most Sarnu minerals and thus comparison of the chondrite-normalised *REE* patterns is a little difficult. However, a plot of the ratios La/Ce verus La/Nd (Fig. 6) serves to illustrate the major points. There is no relative fractionation between 'exsolved' and 'cotectic' carbocernaite (i.e. carbocernaite in Areas A, B, C and D) and the bastnäsite inclusion in carbocer-

TABLE 5
Electron microprobe analyses of carbocernaite and bastnäsite-(La)

	carbocernaite											bastnäsite
Area	B	B	B	C	C	C	C	C	C	C		C
number	1	2	3	4	5	6	7	8	9	10		11
ANALYSIS	W-3	W-4	W	F	H	I	J	T	U	average of 13	sd	
	lamellae in calcite		interstital	large crystals		with britholite		narrow crystals				inclusion in carbocernaite
Na_2O	0.53	0.44	3.83	3.97	4.26	4.84	4.05	4.66	3.65	4.11	0.64	-
MgO	-	-	-	0.23	-	-	-	-	-	-		-
Al_2O_3	-	-	-	-	-	-	0.09	-	-	-		-
CaO	24.21	26.04	17.15	16.28	16.36	15.93	17.10	16.66	17.81	16.95	0.72	0.11
MnO			0.69	0.57	0.37	0.45	0.37	0.35	0.43	0.52	0.16	0.04
SrO	16.01	15.78	18.74	19.67	21.60	20.22	23.33	22.26	23.98	21.36	2.41	0.15
BaO	1.45	1.78	1.64	0.95	1.26	1.24	1.66	1.66	1.64	1.44	0.41	-
La_2O_3	12.40	8.55	13.26	12.67	11.85	12.98	10.41	11.32	9.14	11.77	1.70	32.95
Ce_2O_3	10.68	10.22	10.16	10.32	9.69	10.23	8.67	8.97	8.69	9.72	1.02	23.74
Pr_2O_3	0.64	0.71	0.76	0.88	0.80	0.72	0.65	0.59	0.89	0.75	0.13	1.94
Nd_2O_3	1.75	1.40	1.82	2.07	1.87	1.92	1.89	1.84	2.08	1.98	0.19	5.37
Sm_2O_3	0.44	-	0.31	0.34	0.16	0.17	0.18	0.65	0.30	0.29	0.13	0.26
Eu_2O_3	-	-	-	-	-	-	-	0.16	-	-		-
F	-	-	-	0.21	-	-	-	-	0.27	-		6.55
TOTAL	68.11	64.92	68.36	68.16	68.22	68.70	68.40	69.12	68.88	68.36		71.11
Wt% CO_2*	31.53	31.52	32.02	31.75	31.96	32.56	32.22	32.82	32.15	32.01		35.54
total*	99.64	96.44	100.38	99.91	100.18	101.26	100.62	101.94	101.03	100.37		106.65
					formula to 20 O							formula to 24(O)
Na	0.435	0.368	3.314	3.474	3.757	4.215	3.560	4.053	3.201	3.608		Ca 0.0810
Ca	9.565	9.633	6.686	6.526	6.243	5.785	6.440	5.947	6.799	6.392		Mn 0.0243
total	10.000	10.000	10.000	10.000	10.000	10.000	10.000	10.000	10.000	10.000		Sr 0.0608
												La 12.2917
Ca	1.409	2.385	1.514	1.345	1.728	1.881	1.867	2.059	1.832	1.826		Ce 8.7914
Mg	0.000	0.000	0.000	0.155	0.000	0.000	0.000	0.000	0.000	0.000		Pr 0.7130
Al	0.000	0.000	0.000	0.000	0.000	0.000	0.048	0.000	0.000	0.000		Nd 1.9406
Mn	0.000	0.000	0.261	0.218	0.143	0.171	0.142	0.133	0.165	0.000		Sm 0.0972
Sr	2.544	2.553	3.141	3.334	3.689	3.411	3.972	3.750	4.073	3.631		total 24.0000
Ba	0.240	0.301	0.287	0.168	0.225	0.218	0.299	0.299	0.291	0.255		
La	1.935	1.358	2.182	2.109	1.988	2.150	1.741	1.873	1.525	1.965		F 13.9689
Ce	1.654	1.612	1.600	1.705	1.613	1.682	1.439	1.473	1.439	1.610		
Pr	0.098	0.111	0.124	0.145	0.133	0.118	0.107	0.096	0.147	0.123		
Nd	0.264	0.215	0.290	0.334	0.304	0.308	0.306	0.295	0.336	0.320		
Sm	0.064	0.000	0.048	0.053	0.025	0.026	0.028	0.101	0.047	0.045		
Eu	0.000	0.000	0.000	0.000	0.000	0.000	0.000	0.025	0.000	0.000		
total	8.209	8.535	9.505	9.564	9.847	9.965	9.946	10.096	9.854	9.773		
F	0.000	0.000	0.000	0.300	0.000	0.000	0.000	0.000	0.386	0.000		

* = CO_2 calculated by stoichiometry, and corresponding total
sd = standard deviation
- = below detection limit

naite is also very similar. However, britholite-(Ce) is consistently less light-*REE*-enriched than the other Sarnu minerals. This may be because the britholite-(Ce) represents a different stage of mineralisation, with different relative concentrations of *REE* available from the mineralising fluids and/or it could be that the availability of two (7 and 9-fold coordinated) sites for *REE* in britholite-(Ce) gives rise to a slight crystal chemical preference for the heavier *REE*. Some evidence in favour of the second idea is provided by the much more light-*REE*-enriched normalised

TABLE 6

Electron microprobe analyses of other rare earth minerals: britholite-(Ce), daqingshanite, monazite-(Ce), allanite-(Ce) and REE-rich titanite

	AREA C										AREA E			AREA G
	britholite-(Ce)							daqingshanite			britholite-(Ce)	monazite-(Ce)	allanite-(Ce)	titanite
	representative analyses				average of 9 analyses	sd	average of 5 with carbocernaite	sd	average of 3 at edge of carbocernaite	sd				
	1	2	3	4	5		6		7		8	9	10	11
MgO	-	-	-	-	-		-		-		-	-	1.03	0.58
Al_2O_3	-	-	-	-	-		-		-		-	-	14.21	3.42
SiO_2	24.23	23.98	25.15	23.69	24.20	0.61	23.87	0.40	-		19.85	1.18	31.07	19.64
P_2O_5	0.59	0.59	0.15	2.31	0.89	0.64	0.90	0.31	8.82	0.43	2.08	28.96	-	-
CaO	7.84	7.92	8.00	11.19	8.65	0.96	8.31	0.39	7.75	1.57	10.22	0.34	8.37	2.34
TiO_2	-	-	-	-	-		-		-		-	-	-	15.06
MnO	1.35	1.50	1.48	1.29	1.47	0.25	1.54	0.21	-		1.27	-	3.23	1.22
FeO(T)	-	-	-	-	-		-		-		-	-	12.1	10.06
SrO	1.34	1.50	1.73	1.85	1.79	0.32	1.80	0.42	33.41	1.37	2.94	-	-	0.80
Y_2O_3	0.25	0.25	0.05	0.26	0.24	0.14	0.34	0.09	-		-	-	-	-
BaO	-	-	-	-	-		-		3.17	0.53	-	-	-	-
La_2O_3	16.15	15.58	25.39	20.86	18.87	4.47	15.04	0.82	10.97	1.71	19.89	29.52	11.71	16.66
Ce_2O_3	31.87	31.43	28.31	26.26	29.00	1.86	30.40	1.20	10.91	1.35	31.83	32.34	13.57	22.30
Pr_2O_3	3.18	3.25	1.89	2.35	2.60	0.50	3.01	0.23	-		<1.2	2.07	-	-
Nd_2O_3	10.35	10.36	5.51	6.44	8.42	2.23	10.38	0.46	1.53	0.63	6.10	4.69	-	-
Sm_2O_3	0.91	0.82	0.27	0.62	0.72	0.26	0.93	0.11	-		-	-	-	-
Eu_2O_3	0.21	0.26	-	-	-		0.22	0.05	-		-	-	-	-
Gd_2O_3	0.88	0.86	0.74	0.95	0.87		0.92	0.07	-		-	-	-	-
Dy_2O_3	0.12	-	-	-	0.20		0.20	0.08	-		-	-	-	-
ThO_2	0.12	-	-	-	0.53		0.53	0.34	-		-	-	-	1.63
F	1.27	1.36	1.94	2.26	1.52	0.37	1.24	0.14	n.a.		n.a.	n.a.	n.a.	n.a.
SO_3	-	-	-	-	-		-		0.42	0.08	-	-	-	-
TOTAL	100.66	99.66	100.61	100.33	99.97		99.41		77.29		94.18	99.10	95.34	93.71
O=F,Cl	0.56	0.60	0.86	1.00	0.68		0.55				-	-	-	-
TOTAL	100.10	99.06	99.75	99.33	99.29		98.86		77.29		94.18	99.10	95.34	93.71
	Formula calculated to 25(O)								28(O)		25(O)	24(O)	25(O)	20(O)
Ca	2.215	2.259	2.250	3.066	2.445		2.357	P	3.400	Ca	3.076	Si 0.278	Si 6.232	Si 3.600
Mn	0.302	0.338	0.329	0.279	0.328		0.345	S	0.144	Mn	0.302	P 5.780		Al 0.400
Sr	0.133	0.150	0.171	0.178	0.177		0.179	total	3.544	Sr	0.310	total 6.058		total 4.000
Y	0.035	0.035	0.007	0.035	0.034		0.047			Y	0.000			
Ba	0.000	0.000	0.000	0.000	0.000		0.000	Ca	3.788	Ba	0.000	Ca 0.086	Mg 0.308	Mg 0.159
La	1.571	1.530	2.459	1.968	1.835		1.469	Sr	7.935	La	2.061	La_2O_3 2.570	Al 3.3614	Al 0.338
Ce	3.077	3.063	2.721	2.459	2.800		2.947	Ba	0.567	Ce	3.274	Ce_2O_3 2.795	Ca 6.232	Ca 0.084
Pr	0.306	0.315	0.181	0.219	0.250		0.290	La	1.846	Pr	0.000	Pr_2O_3 0.178	Mn 1.802	Ti 2.595
Nd	0.975	0.985	0.517	0.588	0.793		0.982	Ce	1.823	Nd	0.612	Nd_2O_3 0.395	Fe^{2+} 0.546	Mn 0.189
Sm	0.083	0.075	0.024	0.055	0.066		0.085	Nd	0.249	Sm	0.000	total 6.024	La 0.868	Fe^{2+} 1.542
Eu	0.019	0.024	0.000	0.000	0.000		0.020	total	16.208	Eu	0.000		Ce 0.998	Sr 0.085
Gd	0.077	0.076	0.064	0.081	0.025		0.081			Gd	0.000		total 9.922	La 1.126
Dy	0.010	0.000	0.000	0.000	0.017		0.017			Dy	0.000			Ce 1.496
Th	0.007	0.000	0.000	0.000	0.032		0.032			Th	0.000			Th 0.068
total	8.808	8.849	8.723	8.928	8.801		8.852			total	9.636			total 7.682
P	0.132	0.133	0.033	0.500	0.198		0.201			P	0.495			
Si	6.390	6.383	6.604	6.060	6.381		6.322			Si	5.577			
total	6.522	6.516	6.637	6.560	6.579		6.523			total	6.072			
F	1.059	1.145	1.611	1.828	1.270		1.040			F	0.000			

Analyses 1-6 by WDS, 7-11 by EDS
FeO(T) = total iron as FeO
n.a. = not analysed
- = below detection limits

patterns of monazite-(Ce) and allanite-(Ce) coexisting with britholite-(Ce) at the boundary zone (Area E).

Discussion

A carbonatite?

Although of unusual mineralogy in terms of its mineral compositions, textures and the proportion of *REE* minerals, this rock conforms to the definition of a carbonatite (Le Maitre *et al.*, 1989) because its intrusive relationships are igneous and because it is composed of >50% carbonate minerals. Five further features confirm this identification. (1) The rock is part of a larger suite of carbonatites and associated silicate rocks (Chandrasekaran *et al.*, 1990), the former containing similar minerals to those reported here. (2) The

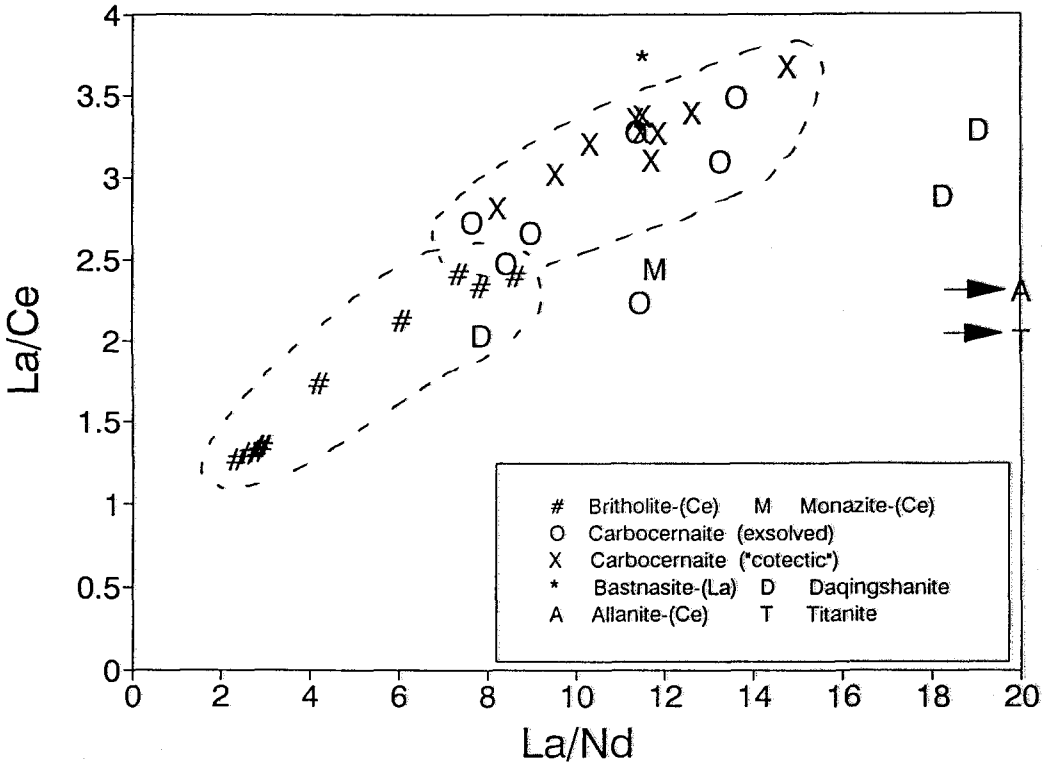

FIG. 6. Plot of chondrite-normalised light *REE* ratios to illustrate the degree of light *REE* enrichment. Middle and heavy *REE* are below electron microprobe detections limits in most Sarnu minerals. The arrows against allanite-(Ce) (A) and titanite (T) indicate the Nd is below detection limit and the La/Nd ratio must be greater than 20. Chondrite values are from Wakita *et al.* (1971). Dashed lines serve to guide the eye to the groups of points. They have no statistical significance.

whole-rock chemistry is consistent with that for carbonatite, but one that is unusually rich in many compatible and incompatible elements (cf. Woolley and Kempe, 1989). (3) The silicate rock bordering the carbonatite is consistent with having been fenitized. (4) All the minerals reported here are known from other carbonatites. (5) The texture of the large calcite crystals, especially in Areas A and B, of smooth crystal boundaries and triple junctions, is typical of sövitic carbonatites.

Comparison with oher carbonatites

REE-rich carbonatites are typically formed in the late stage of carbonatite emplacement. They are often Fe-Mg-rich carbonatites and they usually exhibit secondary textures indicative of formation under hydrothermal or carbothermal conditions [Mariano, 1989). The textures of the majority of *REE* carbonatites contrast markedly with the magmatic textures, indicative of magmatic temperatures, seen in the Sarnu dyke. Therefore, the unusual mineral chemistry of the Sarnu dyke may be linked directly to the unusual conditions of formation: with carbocernaite, Sr-rich calcite, Ca-rich strontianite and Sr-containing baryte at Sarnu in contrast with the more common assemblage of Ca-poor strontianite plus calcite (or frequently, dolomite/ankerite), Fe,Mg oxides, *RE*-minerals and Sr-poor baryte seen at other localities, for example in the Kangankunde and Nkombwa carbonatites, in Malawi and Zambia (Wall, 1991).

Perhaps the best known *REE* carbonatite is the intrusion at Mountain Pass, California (Olsen *et al.*, 1954). Although Mountain Pass and Sarnu are quite different in terms of size, a comparison between the two is useful because Mountain Pass is one of the few carbonatites with evidence of primary crystallisation of major amounts of *REE*. Some of the main carbonatite at Mountain Pass (the Sulfide Queen carbonatite) consists of a calcite carbonatite with an igneous texture comprising phenocrystal Sr-bearing baryte, calcite

(with about 0.4 wt.% SrO) and *RE* fluocarbonates such as bastnäsite, synchisite and parisite. Carbocernaite has not been reported. Experimental work by Jones and Wyllie (1986) predicts that it would be possible to crystallise bastnäsite from a carbonatite melt of Mountain Pass composition at about 600 °C and 1 kbar pressure, conditions not far removed from the >500 °C and 2 kbar suggested for the precipitation of carbocernaite at Sarnu.

The differing mineralogy can be related to differences in bulk chemistry between the two carbonatites. Two components distinguish Mountain Pass from Sarnu: the F and Sr contents. Fluorine is high at Mountain Pass as shown by the abundance of the *RE*-fluocarbonate minerals. In contrast, F is low at Sarnu and mainly restricted to the post-magmatic britholite-(Ce) traversing Areas A, B, C and D (apart from rare inclusions of bastnäsite in carbocernaite). Sr, however, is high at Sarnu and the presence of high levels of Sr in a magmatic environment could be an important factor in favouring the crystallisation of carbocernaite, as well as stabilising the first *REE*-rich carbonate that then underwent exsolution to produce Sr-rich calcite and carbocernaite in Areas A and B. The exsolution textures in the Sarnu carbonates indicate high solubility of Sr and *REE* in the original carbonate melt. It is also noteworthy that the two localities are similar in that both have little apatite and the overall P contents are low.

Interpretation of the textures

Calcite veins, Area G. Since the calcite vein (Area G) in the fenite is cut by the carbonatite dyke it is interpreted as being emplaced first. Furthermore, because the calcite is Sr- and Mn-bearing as typifies carbonatites (Table 3), the vein G can be assumed to record an early manifestation of carbonatite magmatism at this locality. The apatite in the vein could have crystallised from the carbonatite magma with the *REE*-rich rims being formed later, at the same time as the late-stage mineralisation marked by the britholite-(Ce) bands. Alternatively, because both apatite and magnetite are also found as constituents of the fenite, it is possible that they are relicts of the original rock that survived in the carbonate vein but have been affected by later *REE* mineralisation. Ilmenite has been noted elsewhere in the fenite associated with magnetite and may have been a source of titanium for the *REE*-rich titanite.

Areas A, B and E. Areas A and B, which are cut by C, represent the next phase. Since the grain size increases from A to B, it is suggested that A represents the initial and chilled component of this phase. The marginal zone of the fenite in contact with A is altered from the fenitic assemblage of albite + phlogopite to an allanite-(Ce)–britholite-(Ce) assemblage (Area E). The alteration is superimposed on the fenitic assemblage and, therefore, must be later. It could be caused either by the adjacent Area A carbonatite, or by the event that produced the oblique zone of britholite-(Ce) across Areas A, B and C.

The gradual textural transition from A to B with increasing exsolution of carbocernaite is accompanied by increasing *REE* and SrO in the calcite crystallising from the carbonatite magma. For example: successively 6.3, 8.0, 8.8 and 11.2 wt.% SrO is shown in the averaged data of raster analyses in Table 4. The MnO contents remain in the range 3–4 wt.%. The primary calcite that crystallised in Area B is progressively accompanied by the crystallisation of interstitial carbocernaite. This indicates that the carbonatite magma moved compositionally across a field crystallising increasingly Sr,*REE*-rich calcite to a two-phase boundary where carbocernaite also crystallised.

Area C. The large strontian calcite–carbocernaite intergrown crystals of Area C are not believed to be two phases related by exsolution because the texture is markedly different from that between the same two phases in Area B. However, it could be argued that the host phase in Area C was the carbocernaite, and exsolution of Sr-calcite from it produced a texture akin to that seen in perthitic feldspars. Were this the case, such an exsolution texture would be expected in Area D. It is not observed. Symplectic intergrowth can be ruled out because large patches, and sometimes whole crystals, are in optical continuity indicating single crystal growth. In symplectites optical continuity is, in contrast, usually more localised with many centres of crystal growth.

The intergrowth texture of Area C corresponds more closely to micrographic crystallisation of two phases on a cotectic. The elongate or spinifex appearance of the intergrowth in places might suggest rapid crystallisation from a supercooled liquid. In addition, to this intergrowth, there is exsolution of blebs and lamellae of carbocernaite and Ca-rich strontianite from the Sr-calcite probably representing further cooling and/or decrease in pressure. In some calcite crystals this has produced a Ca-strontianite–'low-Sr-calcite' intergrowth (Table 3, Fig. 3*d*).

Since the carbocernaite and Sr-calcite in Area

TABLE 7

Electron microprobe analyses of minerals in fenite (Area F) and calcite vein cutting the fenite (Area G)

	fenite Area F						Calcite vein Area G		
	1	3	2	4	5		6	7	8
	away from calcite vein		phlogopite "green" near calcite vein		albite		apatite FW25	apatite rim FW35	apatite core FW30
SiO_2	39.20	39.42	42.84	36.69	67.15	SiO_2	-	2.91	-
TiO_2	1.92	1.98	0.56	1.42	-	P_2O_5	41.83	37.11	43.02
Al_2O_3	16.04	14.29	12.25	16.53	20.89	CaO	52.71	45.95	51.59
FeO(T)	14.83	13.79	9.79	15.95	0.31	FeO(T)	0.34	-	-
MgO	15.89	17.41	21.43	15.22	-	SrO	0.91	1.61	1.73
CaO	-	-	0.33	0.25	0.59	La_2O_3	-	2.46	-
Na_2O	0.44	-	0.65	0.65	11.01	Ce_2O_3	-	5.22	1.16
K_2O	9.53	9.15	9.08	9.01	-	Nd_2O_3	-	1.96	-
	-	-	-	-	-				
total	97.85	96.04	96.93	95.72	99.95	total	95.79	97.22	97.5
	Mg:Fe 2:1				Ab 97.16				

All analyses are energy-dispersive
FeO(T) = total iron as FeO
- = below detection

C have the same compositions as the late-stage carbocernaite and Sr-calcite in Area B (see Tables 3 and 5), similar crystallisation conditions are envisaged, with the difference that a third phase, Ca-rich strontianite, joined the other two phases in the later stages of crystallisation, followed by baryte and pyrrhotite. Thus the composition of the liquid remaining in the final stages of crystallisation of Area B, was little different from that of the bulk of Area C, indicating a further continuity in the source of the carbonatite magma.

Inclusions of bastnäsite-(La) and thorite in carbocernaite indicate that these minor phases crystallised early.

Summarising, the sequence of crystallisation interpreted for Area C is as follows:

1. Minor bastnäsite-(La) and thorite
2. Cotectic carbocernaite and Sr-calcite, joined later by Ca-rich strontianite.
3. Late-stage magmatic crystallisation of baryte, daqingshanite, and sphalerite. Exsolution to give further carbocernaite, Ca-rich strontianite, and 'Low Sr-calcite".
4. Post-magmatic carbothermal crystallisation of britholite-(Ce) along fracture zone.

Crystallisation of alabandite, Fe-oxides and pyrrhotite is difficult to place within the sequence and appears to have occurred throughout.

Area D. In Area D, the interpretation is similar to that for Area C but with slower cooling causing the more coarse-grained intergrowth of carbocernaite and Sr-calcite, and the more coarse-grained exsolution of carbocernaite from calcite, with the bulk composition remaining approximately the same.

Construction of a phase diagram. A least-squares mixing program, PETMIX (Bryan *et al.*, 1969), was used to calculate the proportions of the phases from the whole rock analysis. The primary carbonate (i.e. the Sr-calcite and the carbocernaite intergrowth) was taken as a single composition (78% by weight), interstitial carbocernaite (2%), Ca-strontianite (1%), pyrrhotite (7%), baryte (2%) and britholite-(Ce) (10%). The components used were SiO_2, FeO, MnO, CaO, SrO, BaO, P_2O_5 and total RE oxides. The sum of squares of residuals was 0.420.

Using data given in Table 4 and the above interpretations, including the deduction that Areas C and D represent cotectic crystallisation, a possible phase diagram can be constructed for a CO_2-saturated system. It is plotted using the wt.% components CaO–(SrO + Ba)-*RE* oxide (Fig. 7). The bulk composition of the whole dyke lies in the Sr-calcite field at point X. The earliest carbonatite recorded here crystallised to give calcite composition G in the <1 mm veins. The first phase of crystallisation in the dyke initially precipitated a calcite richer in Sr, A on Fig. 7, which with progressive fractionation became even richer in Sr and in *REE*, B on Fig. 7. The bulk liquid, however, must have moved along the line B′, since the final crystallisation in Area B is carbocernaite in apparent equilibrium with the Sr-calcite. The calcite, on cooling, intersected a solvus on which carbocernaite was exsolved. Area C would have had a composition such that it coincided with the cotectic between the calcite and carbocernaite fields, point C on Fig. 7. Owing to the sharp discontinuity between Areas B and C, it is possible that C represents a slightly later pulse of magma. It crystallised rapidly, presumably because Area B was relatively cold, and the

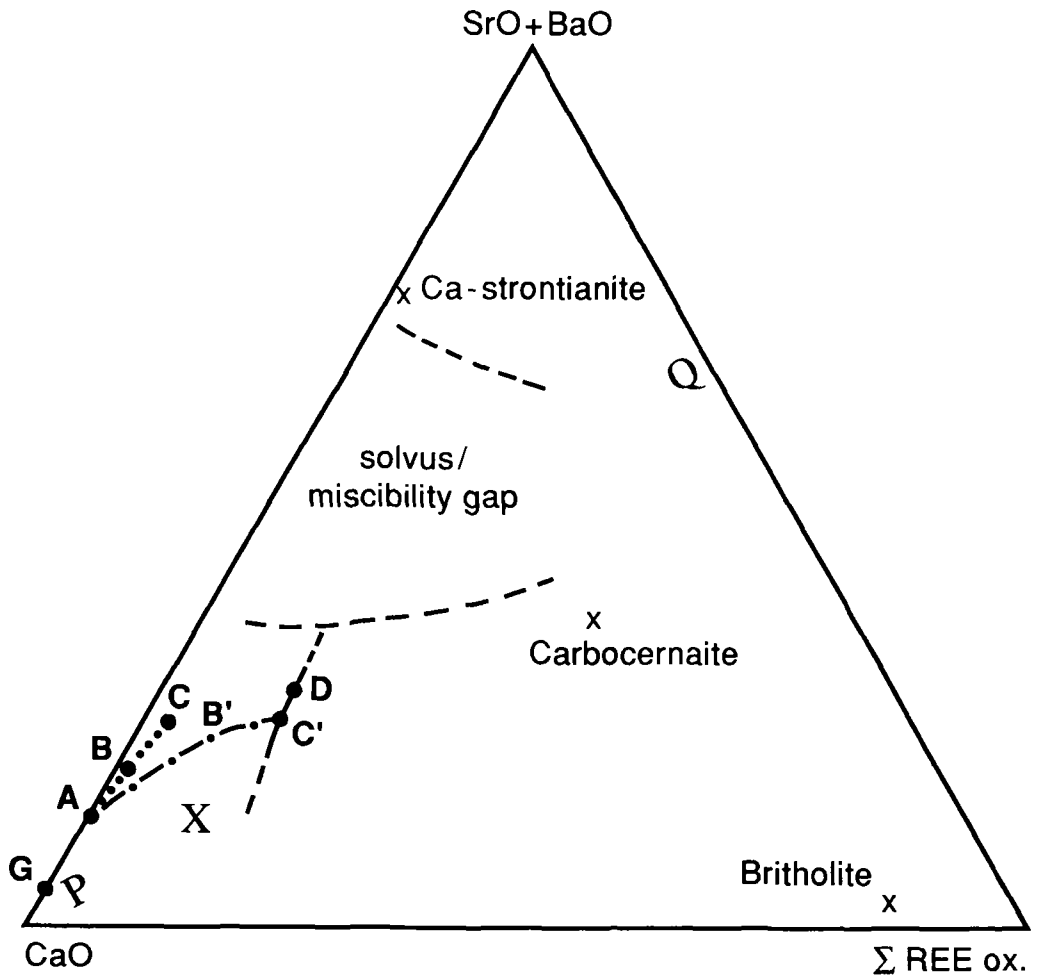

FIG. 7. Sketch of possible phase diagram constructed from the analytical data in terms of wt.% CaO, (SrO + BaO), and Σ*REE* oxides. X = bulk composition of the whole dyke. A, B, C and G correspond to areas on Fig. 2. Dotted line = variation in calcite composition, dash-dot line = inferred change in liquid composition, solid and dash lines = position of cotectic (dashed where inferred). B′, C′ are the calculated liquid compositions, C′ is taken from the bulk analyses from carbonate crystals given in Table 4. PQ is the line of the section given in Fig. 8.

calcite again exsolved carbocernaite on cooling, with strontianite also being exsolved. The subsolidus relations envisaged are sketched on Fig. 8.

Conclusions

1. The Sarnu carbonatite dyke is particularly rich in *REE*, Sr and Ba with 6, 6 and 1.2 wt.% oxide in the bulk rock respectively. The texture of the rock is much easier to see under a scanning electron microscope than under a transmitted light microscope. Detailed electron microprobe analysis and backscattered electron imagery has revealed a complex sequence of crystallisation of strontian calcite, carbocernaite, calcian strontianite and britholite-(Ce).

2. Limits of solid solution between calcite and strontianite, not previously seen in nature, are reported. The calcite has up to 13 wt.% SrO and the strontianite up to 20 wt.% CaO. Comparison with experimental systems suggests conditions of about 500 °C and 2 kbar for crystallisation of high Sr-calcite and high Ca-strontianite and 350 °C and 2 kbar for later low Sr-calcite and high Ca-strontianite.

3. The carbonatite is rare amongst rare-earth-rich carbonatites in having evidence of primary crystallisation of rare earth minerals and believed to be unique in showing evidence of exsolution of a rare-earth-rich phase from a calcium carbonate. The presence of Sr is probably important in stabilising the initial crystallisation of the Sr,*REE*-rich carbonate.

4. Determination of the mineral compositions and interpretation of the beautifully developed textures has allowed a first attempt at the construction of a phase diagram incorporating solvi for calcite, carbocernaite and strontianite and a calcite-carbocernaite cotectic.

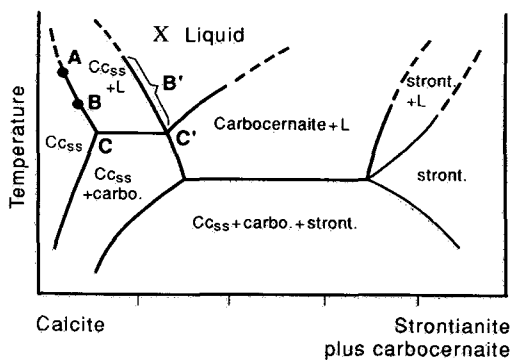

FIG. 8. Sketch of possible pseudobinary system along PQ of Fig. 7. Cc_{ss} = calcite; stront = strontianite; carbo = carbocernatie. X = bulk composition of whole dyke. L = liquid. A, B, and C correspond to areas on Fig. 2 and B′, C′ and the corresponding liquid composition.

Acknowledgements

The authors are grateful to Drs. P. Henderson, A. P. Jones, A. R. Woolley, C. T. Williams and J. W. F. Bowles, who read and improved the manuscript. Thanks to Mr. I. A. Somogyi and J. G. Francis for carrying out the X-ray diffraction analysis and to Mr. G. C. Jones for obtaining an infrared spectrum of carbocernaite.

References

Appleton, J. D., Bland, D. J., Nancarrow, P. H. A., Styles, M. T., Mambwe, S. H., and Zambezi, P. (1992) The occurrence of daqingshanite-(Ce) in the Nkombwa Hill carbonatite, Zambia. *Mineral. Mag.*, **56**, 419–22.

Bryan, W. B., Finger, L. W., and Chayes, F. (1969) Estimating proportions in petrographic mixing equations by least-squares approximation. *Science*, **163**, 926–7.

Bulakh, A. G., Kondrat'eva, V. V., and Baranova, E. N. (1961) Carbocernaite, a new rare earth carbonate. [*Zapisiki Vses. mineral. Obsch.*, **90**, 42–9 (in Russian)]; Abstr. In New Mineral Names. *Am. Mineral.*, **46**, 1202.

Carlson, W. D. (1980) The calcite–aragonite equilibrium: effects of Sr substitution and anion orientational disorder. *Am. Mineral.*, **65**, 1252–62.

Chandrasekaran, V., Srivastava, R. K., and Chawade, M. P. (1990) Geochemistry of the alkaline rocks of Sarnu-Dandali area, district Barmer, Rajasthan, India. *J. Geol. Soc., India,*, **36**, 365–82.

Chang, L. L. Y. and Brice, W. R. (1972) Subsolidus phase relations in aragonite-type carbonatites: II. The systems $CaCO_3$–$SrCO_3$–$PbCO_3$ and $CaCO_3$–$BaCO_3$–$PbCO_3$. *Am. Mineral.*, **57**, 155–68.

Clark, A. M. (1984) Mineralogy of the Rare Earth Elements. In *Rare Earth Element Geochemistry*. (Henderson, P., ed), Elsevier, Amsterdam, 33–61.

Clarke, L. B., Le Bas, M. J., and Spiro, B. (1992) Rare earth, trace element and stable isotope fractionation of carbonatites at Krudfontein, Transvaal, S. Africa. *International Kimberlite Conference, 5 Araxá 1991. Proceedings*. CPRM Special publication. CPRM, Brasília (in press).

Exley, R. A. (1980) Microprobe studies of *REE*-rich accessory minerals: implications for Skye granite petrogenesis and *REE* mobility in hydrothermal systems. *Earth Planet. Sci. Lett.*, **48**, 97–110.

Jones, A. P. and Wyllie, P. J. (1986) Solubility of rare earth elements in carbonatite magmas, indicated by the liquidus surface in $CaCO_3$–$Ca(OH)_2$–$La(OH)_3$ at 1 kbar pressure. *Appl. Geochem..*, **1**, 95–102.

Le Bas, M. J. and Srivastava, R. K. (1989) The mineralogy and geochemistry of the Mundwara carbonatite dykes, Sirothi District, Rajasthan, India. *Neues Jahrb. Mineral., Abh.*, **160**, 207–27.

Le Maitre, R. W., Bateman, P., Dudek, A., Keller, J., Lameyre, J., Le Bas, M. J., Sabine, P., Schmid, R., Sørensen, H., Streckeisen, A., Woolley, A. R., and Zanettin, B. (1989) *A Classification of Igneous Rocks and Glossary of Terms*. Blackwell, London, pp. 193.

Mariano, A. N. (1989) Nature of economic mineralisation in carbonatites and related rocks. In *Carbonatites: genesis and evolution* (Bell, K., ed.). Unwin Hyman, London, 149–76.

Nash, W. P. (1972) Apatite chemistry and phosphorous fugacity in a differentiated igneous intrusion. *Am. Mineral.*, **57**, 877–86.

Olsen, J. C., Shawe, D. R., Pray, L. C., and Sharp, W. N. (1954) Rare-earth mineral deposits of the Mountain Pass district, San Bernadino County, California. *U.S. Geological Survey Professional paper*, **261**, 75 pp.

Srivastava, R. K. (1977) A comprehensive atomic absorption and spectrophotometric scheme for the determination of major and trace elements in rocks and minerals. *Neues Jahrb. Mineral., Abh.*, **9**, 425–32.

Wakita, H., Rey, P., and Schmitt, R. A. (1917) Abundances of the 14 rare earth elements and 12 other elements in Apollo 12 samples: five igneous and one breccia rocks and four soils. *Proc. 2nd Lunar Sci. Conf., Geochim. Cosomochim. Acta, Suppl.*, **2**, 1319–29.

Wall, F. (1991) Comparison of element distribution in rare earth rich rocks from the Kangankunde and Nkombwa Carbonatite Complexes. *International Kimberlite Conference, 5 Araxá 1991. Extended abstracts*. CPRM Special publication, 2/91. CPRM, Brasília, 446–7.

Woolley, A. R. and Kempe, D. R. C. (1989) Carbonatites: nomenclature, average chemical compositions, and element distribution. In *Carbonatites: genesis and evolution* (Bell, K., ed.). Unwin Hyman, London, 1–14.

Wood, D. A., Joron, J. L., and Treuil, M. (1979) A reappraisal of the use of trace elements to classify and discriminate between magma series erupted in different tectonic settings. *Earth Planet. Sci. Lett.*, **45**, 326–36.

Wyllie, P. J. (1989) Origin of carbonatites: evidence from phase equilibria studies. In *Carbonatites: genesis and evolution* (Bell, K., ed). Unwin Hyman, London, 500–45.

[*Manuscript received 14 May 1992: revised 15 September 1992*]